Results and Discussion

Chapter IV

Adsorption Studies Employing PJBAC

Results of varied experiments verified for chosen dyes and copper ion are explained in this chapter.

4.1 BET and BJH Analyses

The adsorption performance of any system mostly depends on the internal pore structure. Pore sizes classified according to International Union of Pure and Applied Chemistry declare the range d<20 Å to be micropores, 20 Å < d< 500 Å to be mesopores and d > 500 Å to be macropores[119]. PJBAC was found to be mesoporic in nature after phosphoric acid activation process which was confirmed by 283.4 Å predominantly, as their pore diameter lie in the range of 20 Å < d < 500 Å. The linearity of BET plot (Figure 4.1) indicates prominent surface area and pore size distribution in favour of mesoporous and macroporous materials (Table 4.1). BJH analysis is employed to determine specific pore volume based on the pattern of lines as shown in figure 4.2. Figure 4.3 depicts a typical N_2 sorption isotherm indicative of adsorption and desorption curves. The hysteresis loop observed between the lower adsorption and upper desorption curves implies the existence of mesoporosity.

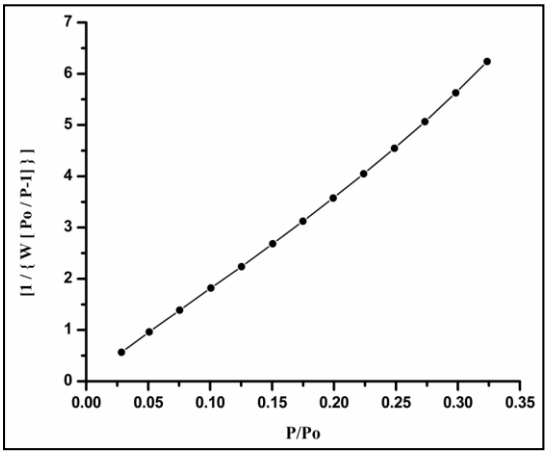

Figure 4.1 BET plot

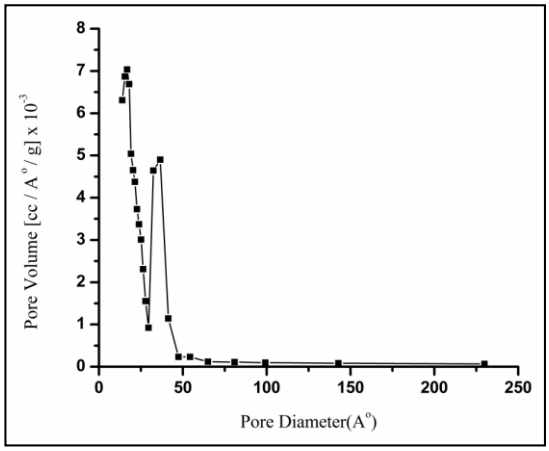

Figure 4.2 BJH plot

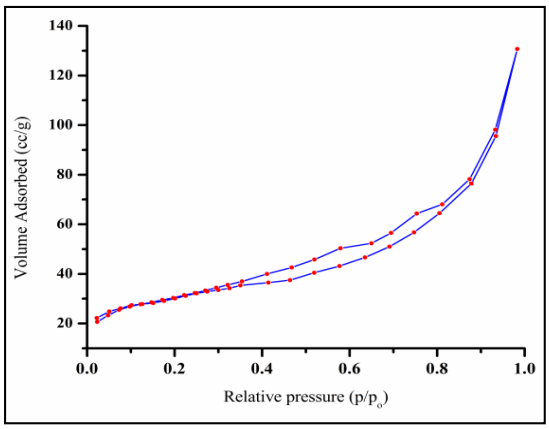

Figure 4.3 Adsorption/Desorption Isothermal Plot

4.2 Physico- Chemical Characterisation

The physico-chemical parameters of PJBAC are listed in Table 4.1. It is obvious from the table that the apparent density value of PJBAC is 0.52 which describes the carbon grade determination. Activated carbons with a random arrangement of micro-crystallites and relatively low apparent density exhibit a strong cross-linking system. Also, it is reported that the fine sized carbons having an apparent density in the range of 0.25 -0.75 g/mL[120] exhibit effective sorption of dyes and heavy metal ions. The low bulk density value supports the presence of large number of pores in PJBAC and in turn 7.2% moisture content of PJBAC implies least influence on its adsorptive power[121]. 4.8% ash content is indicative of presence of inorganic constituents in trace amounts. The low acid value and water soluble matter corresponds to the insolubility of carbon in acids/water, thereby facilitating its utility in the analysis of acidic/alkaline nature of dye wastewaters.

Zero point charge (pH_{ZPC}) is of fundamental importance in surface science, explaining the ability of the sorbent to adsorb harmful ions from aqueous solutions. The neutral pH_{ZPC} value (Table 4.1) supports the extensive sorption nature of PJBAC towards toxic cations and anions[122]. The percentages of C, H, N and S elements registered higher carbon content against other elements.

Appreciable iodine number (757mg/g) and methylene blue number (588mg/g) values suggest high degree of activation/ uptake of dye molecules based on PJBAC

suitability[123]. Notable porosity value emphasizes effective sorptive nature[124]. It is related to the bulk density and specific gravity of PJBAC. A comparison table 4.1a of PJBAC against other sorbents show the carbon under study is found to possess better sorption properties.

Table 4.1 Physico - Chemical Characterisation of PJBAC

Properties	**PJBAC**
pH of 1 % solution	6.68
Conductivity	0.15
Ash content (%)	4.8
Moisture (%)	7.2
Volatile matter (%)	19.1
Acid soluble matter (%)	1.7
Water soluble matter (%)	2.1
Bulk density (g/mL)	0.52
Specific gravity	1.54
Porosity (%)	53.10
Methylene blue value (mg/g)	588
Iodine number (mg/g)	757
PHzpc	6.3
Surface area (m^2/g)	385.2
Mean Pore diameter (A^o)	28.6
Carbon (%)	61.43
Hydrogen (%)	2.99
Nitrogen (%)	1.00
Sulphur (%)	Nil
Oxygen (%)	39.78
Fixed carbon (%)	68.1
Yield (%)	73.6
Surface acid groups	
Phenolic	0.84
Carboxylic	1.18
Lactonic	0.41

Table 4.1a Characteristics Comparison with Reported Literature

Adsorbents	Ash (%)	Moisture (%)	Volatile Matter (%)	Fixed Carbon (%)
Moringa oleifera bark[125]	11.1	12.5	66.5	20.1
hazelnut husk[126]	0.47	3.88	18.44	78.21
Holm oak corn[127]	2.5	7.5	70.6	48.7
Waste printed circuit boards[128]	6.6	2.63	23.47	67.3
Cordia sebestena[129]	17.8	5.4	18.9	57.9
Mango seed[130]	2.33	15.47	26.79	55.41
Apple peel[131]	7.43	12.27	72.8	7.4
Cashew nut shell[132]	2.75	9.83	65.4	22.21
Holm oak[133]	2.3	9.5	80.8	7.4

4.3 Morphological Studies

4.3.1 SEM and EDAX Analyses

SEM images of raw material, activated carbon and loaded carbons are shown in figures 4.4-4.8. Porous morphology of activated carbon (Figure 4.5) against the precursor (Figure 4.4) supports the enhancement of the sorption characteristics of the former. Smoothening of unoccupied pores (Figures 4.6-4.8) and disappearances at certain points favour the adsorption of dyes and metal ion.

Appearance of new peaks at 2 and 8 keV correspond to uptake of Cu(II) by PJBAC (Figure 4.10), being absent in the activated carbon spectra (Figure 4.9).

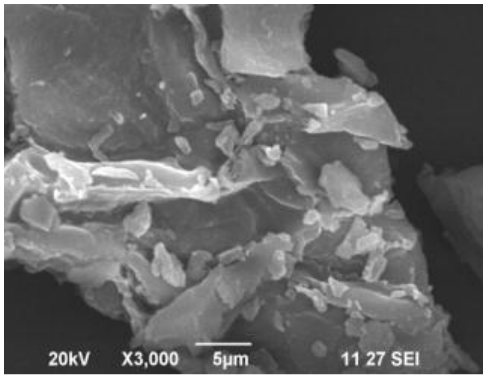

Figure 4.4 SEM Image - Raw PJB

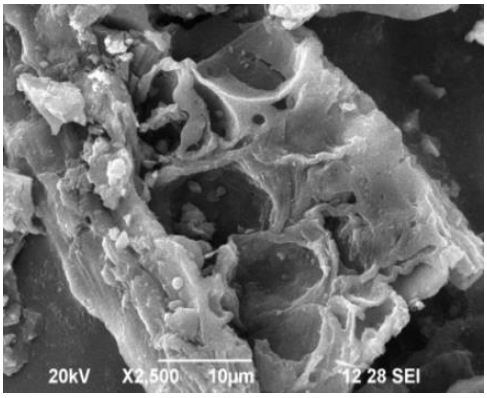

Figure 4.5 SEM Image - Unloaded PJBAC

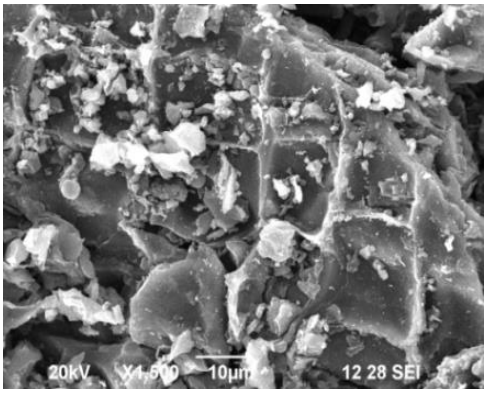

Figure 4.6 SEM Image - DB2 Loaded PJBAC

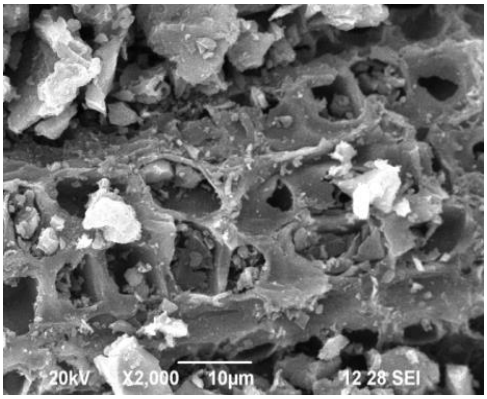

Figure 4.7 SEM Image - RR152 Loaded PJBAC

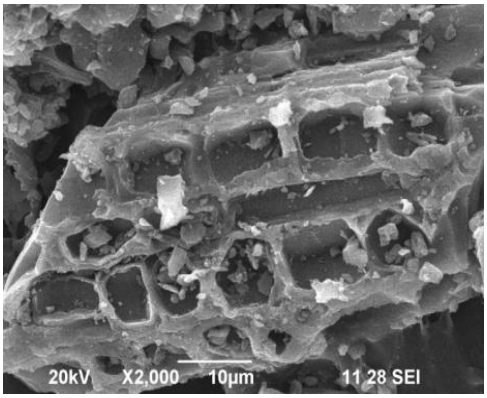

Figure 4.8 SEM Image - Cu(II) Loaded PJBAC

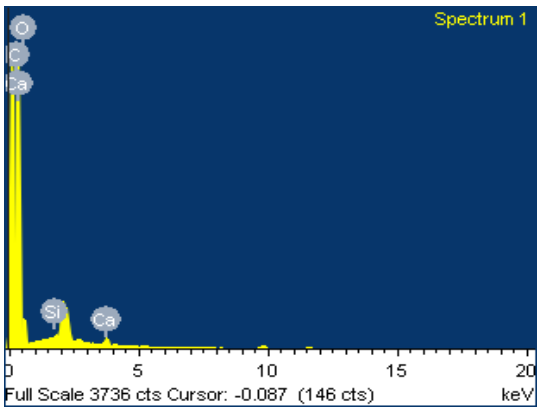

Figure 4.9 EDAX Spectra - Unloaded PJBAC

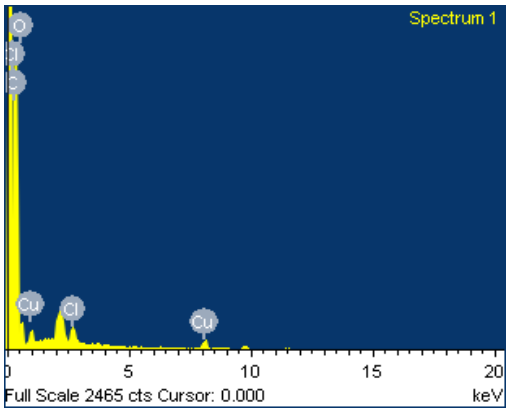

Figure 4.10 EDAX Spectra - Cu(II) Loaded PJBAC

4.3.2 FTIR Spectral Studies

FTIR spectra of dyes/Cu(II) loaded PJBAC samples are presented in figure 4.11. The peak position at 3747 cm^{-1} corresponding to 4.11a indicates that the stretching vibration of OH group and the one about 2322 cm^{-1} shows the presence of alkyl group or tannin. The peaks at 1575 cm^{-1}, 1324 $cm^{-1}$and 1162 cm^{-1} corresponds to C-C bond in aromatic conjugation, C–N peptide bond and S,O interaction respectively[134].The shifts and respective changes in the peaks at 1324 cm^{-1}, 1167 cm^{-1}, 3714 cm^{-1} and 1345 cm^{-1} for the loaded counterparts imply the involvement of functional groups during adsorption process.

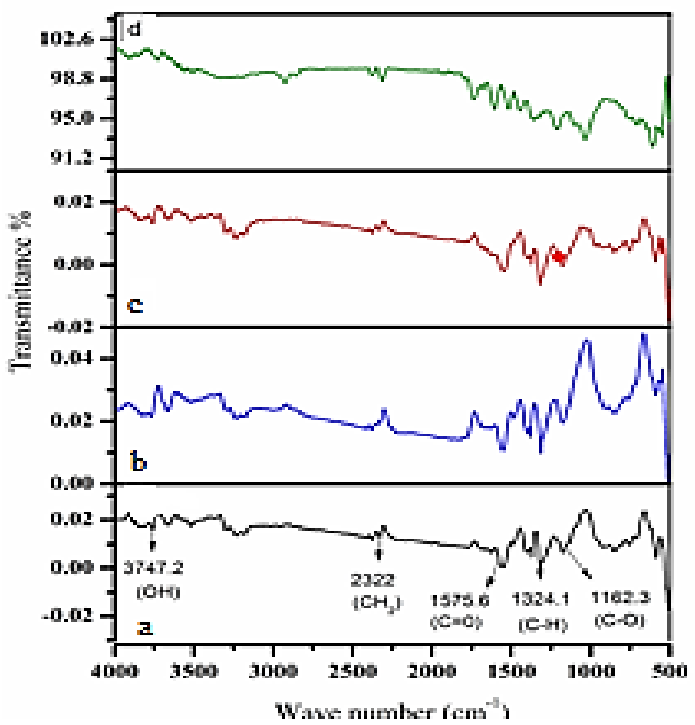

Figure 4.11 FT-IR Spectra of (a) Unloaded PJBAC, (b) DB2 Loaded PJBAC, (c) RR152 Loaded PJBAC and (d) Cu (II) Loaded PJBAC

4.3.3 TGA-DSC Analysis

Thermal decomposition curve of PJBAC (figure 4.12) indicates a significant weight loss at temperature < 120^{o} C which may be due to the evaporation of moisture content. The stages corresponding to weight loss can be attributed to the factors of releasing volatiles and decomposing lignins from 600^{o}C to 1000^{o}C implied by gradual declination of the curve.

The DSC curve in figure 4.12 refer to a slight endothermic region between 26^{o}C and 125^{o}C corresponding to evaporation of water. A steep rise in the curve from 125^{o}C to 400^{o}C is indicates cellulose/hemicelluloses decomposition accompanied by release of heat. The maximized curve at 450^{o}C may refer to vaporisation of certain organic compounds. A decline in the curve beyond 500^{o}C shall suggest pyrolysis of lignin and degradation of carbonaceous structure upto 1000^{o}C.

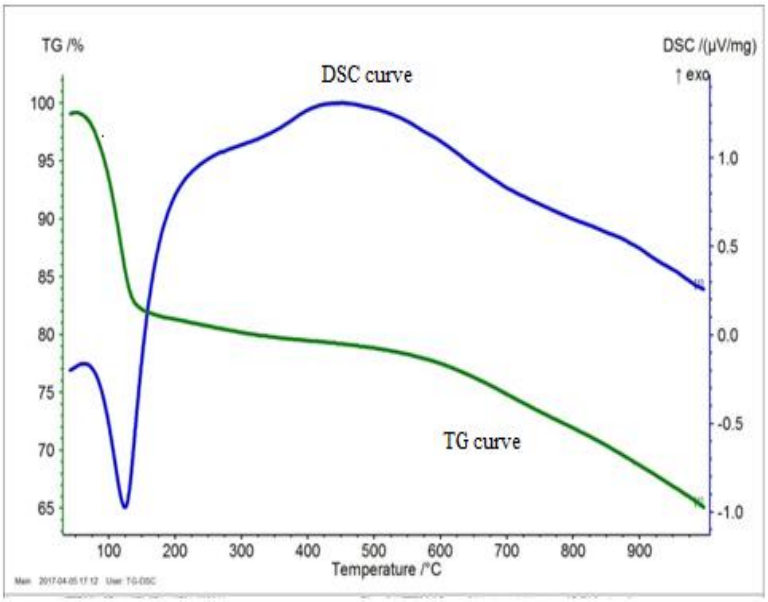

Figure 4.12 TGA- DSC Curve - PJBAC

4.4 Effect of Initial Concentration and Contact Time

The amounts of dyes and divalent ion adsorbed by PJBAC are tabulated in tables 4.2-4.4 and the corresponding curves are represented in figures 4.13- 4.15 respectively. Rapid uptake of dyes and Cu(II) ion had occurred initially upto 10 minutes then slowed down and attained an equilibrium at 60 minutes, 30 minutes and 18 minutes for DB2, RR152 and Cu(II) respectively. This trend could be due to the easy availability of free active sites at the beginning of the adsorption process, whereas after a specific period of time active sites will be gradually occupied slowing down the adsorption process[135] as evident from the smooth dynamic equilibrium curves.

The experimental results reveal that the removal percentage of DB2, RR152 and Cu(II) diminish with increase in concentration, whereas the actual amount of adsorption of DB2, RR152 and Cu(II) per unit mass of adsorbent increases. This may be due to an increase in the driving force of concentration gradient to overcome the mass transfer resistance of the adsorbate between solution and solid phases by increase in concentration of the adsorbate molecule[136].

Table 4.2 Effect of Initial Concentration and Contact Time - DB2

System	Time (min)	Amount Adsorbed (mg/g)					
		25mg/L	50 mg/L	75 mg/L	100 mg/L	125 mg/L	150 mg/L
DB2-PJBAC	10	9.4	18.1	26.1	36.1	40.5	46.45
	20	9.7	18.7	27.7	37.6	43.8	48.3
	30	10.4	19.9	28.9	39.8	45.4	50.4
	40	10.8	20.8	30.4	42.1	46.6	54.6
	50	11.3	22.3	32.4	46.2	49.4	58.3
	60	11.9	23.5	34.5	49.2	60.0	66.4
	90	11.9	23.5	34.5	49.3	60.2	66.4

Adsorbent dose 100 mg; Agitation time: 60 min; pH: 6; Temperature: 303K.

Table 4.3 Effect of Initial Concentration and Contact Time - RR152

System	Time (min)	Amount Adsorbed (mg/g)					
		25mg/L	50 mg/L	75 mg/L	100 mg/L	125 mg/L	150 mg/L
RR152-PJBAC	10	5.2	11.2	16.6	21.5	26.3	30.1
	20	5.8	11.8	17.2	22.3	26.7	31.5
	30	6.0	12.1	17.9	23.5	28.9	33.3
	40	6.1	12	16.5	22.6	28.2	32.2
	50	6.2	11.8	16.8	23.1	27.0	32.1
	60	6.0	11.8	15.7	23.6	27.9	33.0

Adsorbent dose 150 mg; Agitation time: 30 min; pH: 6; Temperature: 303K.

Table 4.4 Effect of Initial Concentration and Contact Time - Cu(II)

System	Time (min)	Amount Adsorbed (mg/g)				
		4 mg/L	8 mg/L	12 mg/L	16 mg/L	20 mg/L
Cu(II)-PJBAC	3	1.92	4.29	7.86	10.33	14.86
	6	2.06	4.40	8.08	10.62	15.72
	9	2.58	5.21	8.42	11.68	15.89
	12	3.02	5.92	8.97	11.94	16.24
	15	3.29	6.43	9.34	12.23	16.90
	18	3.31	6.42	9.42	12.90	17.10
	21	3.31	6.57	9.74	12.72	17.10
	24	3.31	6.56	9.73	12.70	17.10

Adsorbent dose 60 mg; Agitation time: 18 min; pH: 6; Temperature: 303K.

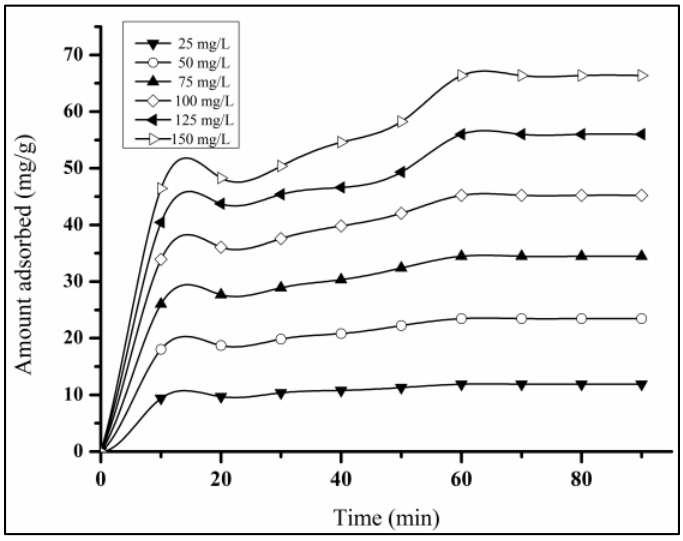

Figure 4.13 Effect of Initial Concentration and Contact Time - DB2

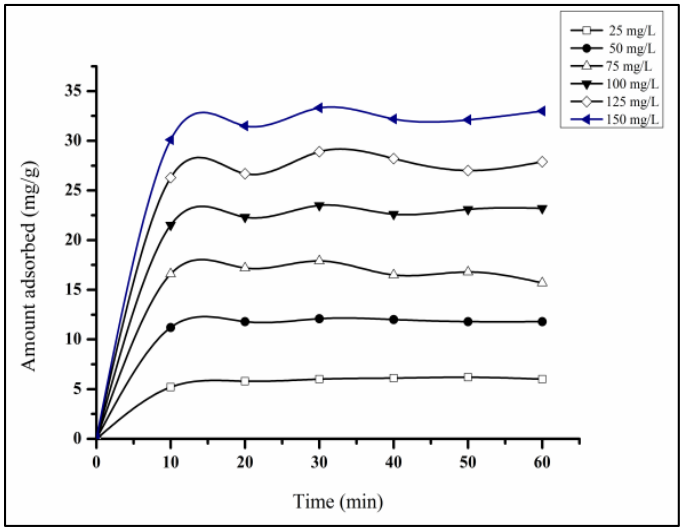

Figure 4.14 Effect of Initial Concentration and Contact Time – RR152

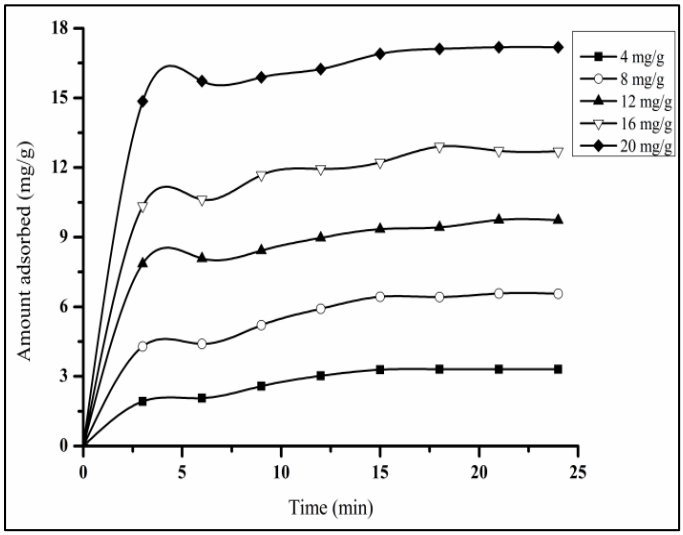

Figure 4.15 Effect of Initial Concentration and Contact Time - Cu(II)

4.5 Effect of Dosage

Figures 4.16, 4.17 and 4.18 shows that influence of the carbon dose on the removal of where the removal of toxic dyes and Cu(II) ion. Approximately 95% removal of DB2, RR152 and Cu(II) is achieved at dosages of 100,150 and 60 mg respectively, is calculated from the smooth, continuous curves. The corresponding values are listed in tables 4.5-4.7. The rate of adsorption was insignificant with further increase in dosage,

due to the overcrowding of carbon particles, available for sorbate species being termed as solid concentration effect.

Table 4.5 Effect of Dosage - DB2

Contact Time (min)	Percentage of Adsorption			
	50 mg	**100 mg**	**150 mg**	**200 mg**
10	55.4	67.8	65.8	60.8
20	59.4	72.1	71.2	70.1
30	61.6	75.2	73.1	65.2
40	63.8	82.6	72.4	69.6
50	65.1	88.1	75.5	79.1
60	68.1	96.7	88.4	83.4
90	68.2	96.4	85.2	83.0

Dye concentration: 100 mg/L; Agitation time: 60 min; pH: 6; Temperature: 303K.

Table 4.6 Effect of Dosage -RR152

Contact Time (min)	Percentage of Adsorption				
	50 mg	**100 mg**	**150 mg**	**200 mg**	**250 mg**
10	60.5	71.1	83.3	82.6	75.2
20	62.7	75.7	91.0	87.5	76.5
30	68.0	76.0	94.4	89.5	82.5
40	67.4	74.0	93.1	89.5	79.8
50	68.0	75.0	94.4	87.9	78.5

Dye concentration: 100 mg/L; Agitation time: 30 min; pH: 6; Temperature: 303K.

Table 4.7 Effect of Dosage - Cu(II)

Contact Time (min)	Percentage of Adsorption				
	20 mg	**40 mg**	**60 mg**	**80 mg**	**100 mg**
3	22.58	42.30	64.84	62.86	60.61
6	32.62	48.49	76.11	70.35	63.35
9	35.00	55.38	83.22	77.5	71.75
12	43.76	63.39	85.32	81.76	75.76
15	44.72	69.16	89.32	82.84	77.84
18	51.96	74.26	94.18	87.14	74.14
21	51.96	74.31	94.18	86.13	74.01
24	51.82	74.10	94.12	86.4	74.12

Metal ion concentration: 20 mg/L; Agitation time: 18 min; pH: 6; Temperature: 303K.

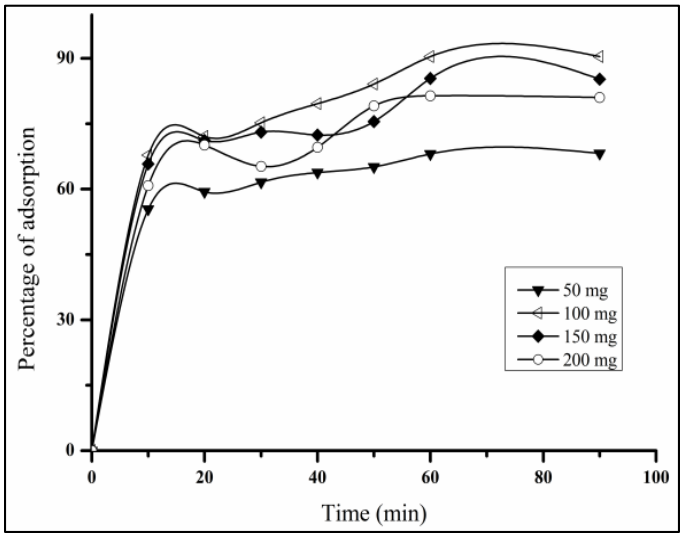

Figure 4.16 Effect of Dosage -DB2

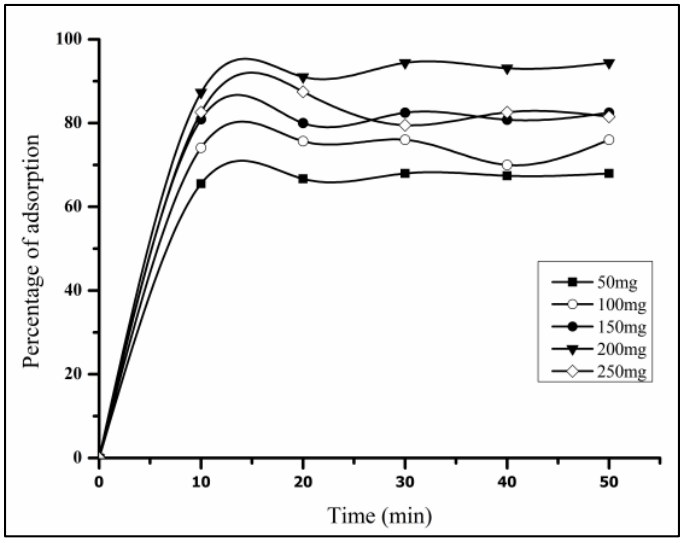

Figure 4.17 Effect of Dosage - RR152

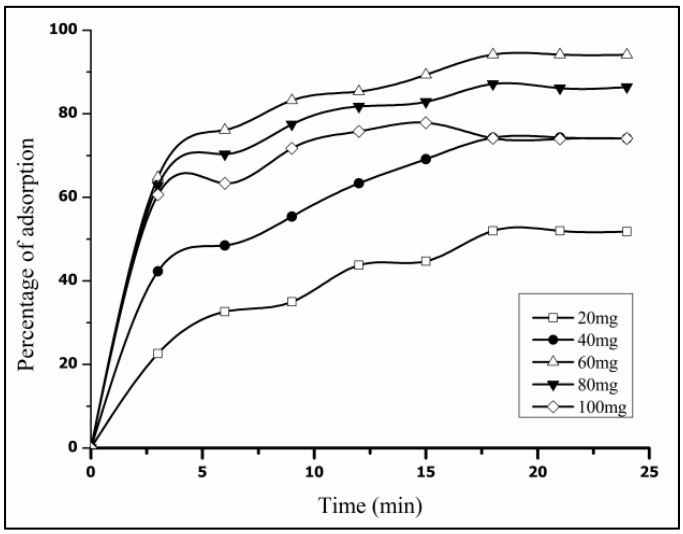

Figure 4.18 Effect of Dosage - Cu(II)

4.6 Effect of pH

The influence of pH on the removal of DB2 and RR152 from aqueous solutions is depicted in figure 4.19, where the maximum removal of dyes (98.6% -DB2 and 99.6%- RR152) had occurred at pH 2.The percentage removal of the dyes decreased slowly with rise in the initial pH of the solution from 4-10 (Table-4.8). It is obvious that at lower pH values, higher sorption had occurred, the reason probably being the positive charge of the sorbent surface, due to the protonation of functional groups present in the

activated carbon, favouring the adsorption. Another assumption could be the impulsive electrostatic attraction between the dye anions and sorption sites at acidic pH. In turn, at higher pH, greater is the availability of negatively charged sites, due to the electrostatic repulsion between dye anions and PJBAC, reflecting in the diminishing nature of sorption. Also, in alkaline pH, the number of OH^- ions on the adsorbent surface significantly competes with dye molecules thereby getting sorbed on carbon surface prior to the latter[137, 138]. A similar trend was observed in the adsorption of dyes onto activated carbon derived from peanut shell[139] and papaya seeds[140].

The Cu(II)-PJBAC system registered higher adsorption with rise in pH upto pH 6, followed by a decline beyond, indicative of inverted parabola (Figure 4.20). Acidic solution (low pH) inhibits metal uptake because of the high concentration of H^+ ions competing with Cu(II) ions due to the protonation of various functional groups (carboxylic and phenolic) present on the PJBAC surface.

Table 4.8 Effect of pH

System	Contact Time (min)	Adsorbent Dose (mg)	Percentage of adsorption				
			pH 2	pH 4	pH 6	pH 8	pH 10
DB2-PJBAC	60	100	98.6	97.2	96.4	76.2	62.8
RR152-PJBAC	30	200	99.6	95.7	94.4	80.3	55.8
Cu(II)-PJBAC	18	60	29.6	77.8	94.2	47.9	21.6

Concenration: 100mg/L (DB2); 100mg/L (RR152); 20mg/L: Cu(II); Temperature: 303K.

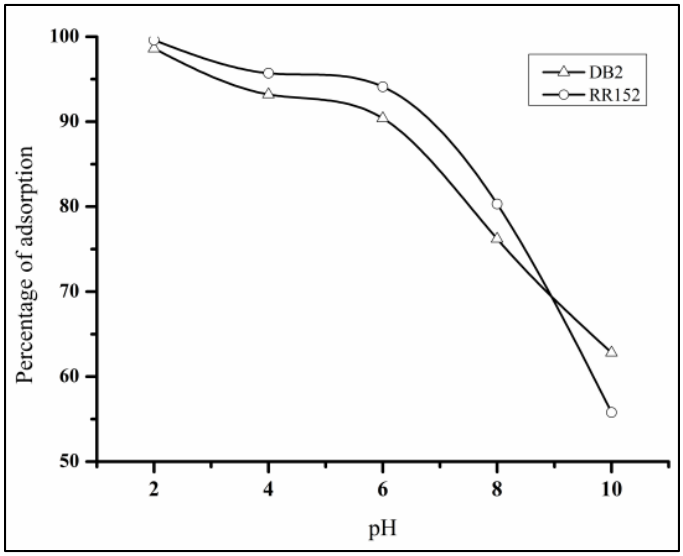

Figure 4.19 Effect of pH - DB2&RR152

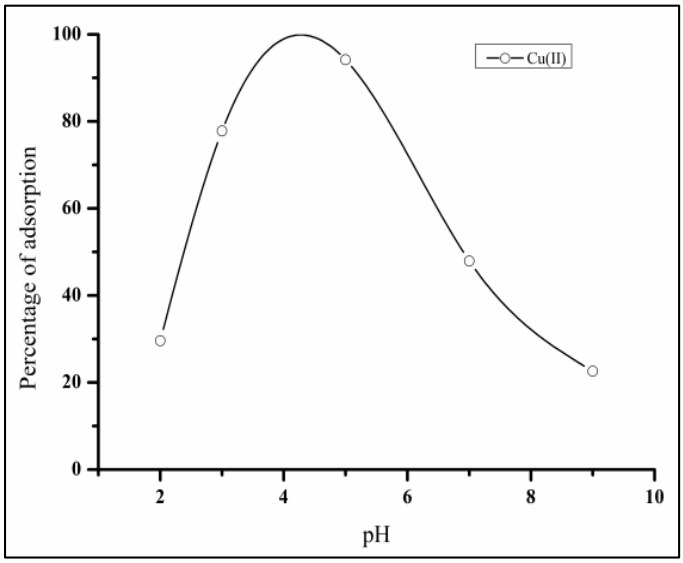

Figure 4.20 Effect of pH - Cu(II)

4.7 Effect of Temperature

A plot of three sorption systems at variable temperature environments is shown in figure 4.21. An inverse relation between the % removal and temperatures is evident from the dripping lines favoured by the listed values (Table 4.9) ranging from 96.6% to 87.9% for temperatures 303K to 333K respectively. This may be attributed to the weakening of the bonds between the dye molecules and the active sites of PJBAC at higher

temperatures[141]. Also, the increase in kinetic energy of sorbate species at higher temperatures may cause the former to unbind themselves from solid surface into the prepared aqueous solutions. The above statement is supported by Raji et.al., and Anirudhan et.al., for Hg(II) removal using saw dust[142] and coconut coir pith[143]. The observations made suggest that removal of DB2, RR152 and Cu(II) by PJBAC is a kinetically controlled process in an exothermic fashion.

Table 4.9 Effect of Temperature

System	Conc. of the solution (mg/L)	Adsorbent dose (mg)	Percentage of adsorption			
			303 K	313K	323K	333K
DB2-PJBAC	100	100	96.6	89.5	89.1	87.9
RR152-PJBAC	100	150	94.7	93.8	92.6	91.7
Cu(II)-PJBAC	20	60	94.9	93.5	92.0	89.7

Contact time: 60 min (DB2); 30 min (RR152); Cu(II): 18 min; pH: 6

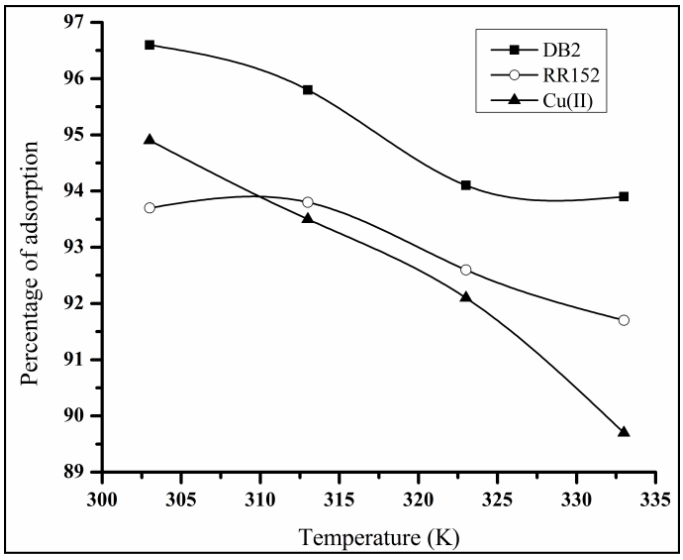

Figure 4.21 Effect of Temperature

4.8 Effect of Cations/ Anions/ Co-ions

The influences of various cations/anions/co-ions on the removal of Cu(II) from aqueous solutions listed in table 4.10. A marked inhibition in % removal is observed for Mg^{2+} cation (74.7% against 95.1%) at standardized initial concentration in preference to other ions, where only appreciable influence is registered. This can be explained in terms of ionic radii, Mg^{2+} (0.72 Å) being smaller than K^+ (1.38Å) and Na^+(1.02Å) has greater degree of hydration, thereby the hydrated ionic radii is in the order: $Mg^{2+}>Na^+>K^+$. The smaller hydrated ionic radii of a cation lead to decrease in the swelling pressure within the PJBAC matrix, in turn exposing to greater affinity of sorbent surface towards Mg^{2+}. Similarly, chloride anion is found to inhibit Cu(II) uptake which may be due to the preferential formation of chloro complex ($CuCl_2$) more than that of NO_3^- influence. The chosen co-ions [Cr(VI) and Zn(II)] registered minimal inhibition supporting the efficiency of PJBAC in trapping Cu(II) ions amidst these environments.

Table 4.10 Effect of Cations/ Anions/ Co-ions - Cu(II)

% removal of Cu^{2+} in the absence of ions	Percentage o f adsorption							
	Conc (mg/L)	Cations			Anions		Co-ions	
		Mg^{2+}	Na^+	K^+	Cl^-	NO_3^{2-}	Zn^{2+}	Cr^{6+}
95.1	100	74.70	82.04	88.20	79.10	87.20	92.40	89.30
	200	72.90	80.14	87.13	77.14	86.50	91.40	87.91
	300	71.70	78.22	86.33	74.87	84.24	90.23	86.30
	400	69.70	75.34	84.45	73.05	82.35	89.40	85.80
	500	67.70	72.46	82.37	70.28	80.63	88.70	84.42

Metal ion concentration: 20 mg/L; contact time: 18 min; pH:6 ; Temperature: 303K

4.9 Desorption and Regeneration studies

Desorption and regeneration values are represented through graph and bar charts respectively (Figure 4.22-4.25). Increase in concentration of desorbing medium reflected

in the decline of desorption in all the three cases, thus indicating 0.01M HCl registered a maximum of 90% recovery.

The adsorption/desorption cycles show the amounts of DB2 and RR152 adsorbed by PJBAC and their consecutive desorption, wherein a relative diminishing factor is established. But in the case of Cu(II), the amounts adsorbed are 17.13, 11.34 and 6.87 mg/g against the amounts desorbed, being 50.93, 36.53 and 29.37 mg/g, favouring better regenerating capacity of Cu(II)- PJBAC system.

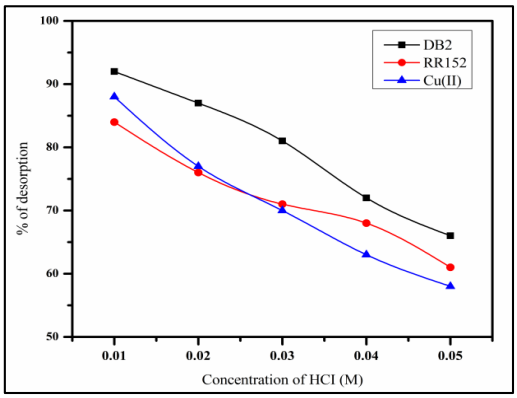

Figure 4.22 Desorption plot

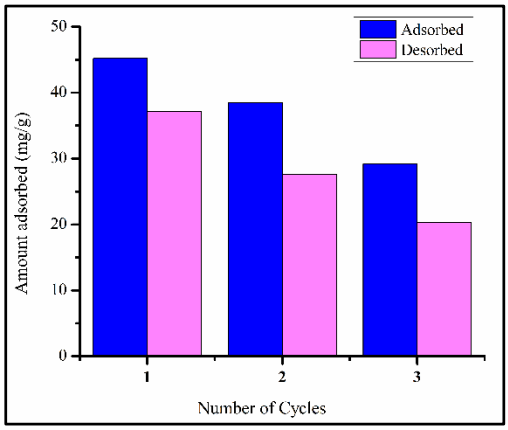

Figure 4.23 Regeneration - DB2

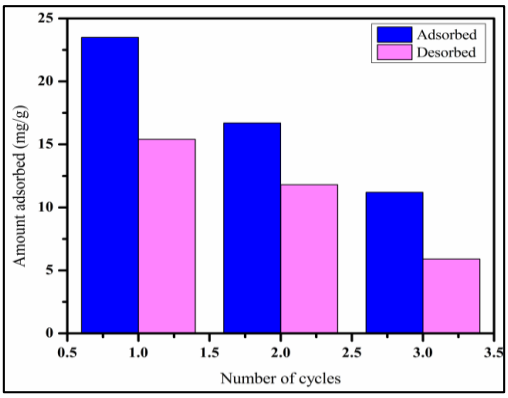

Figure 4.24 Regeneration - RR152

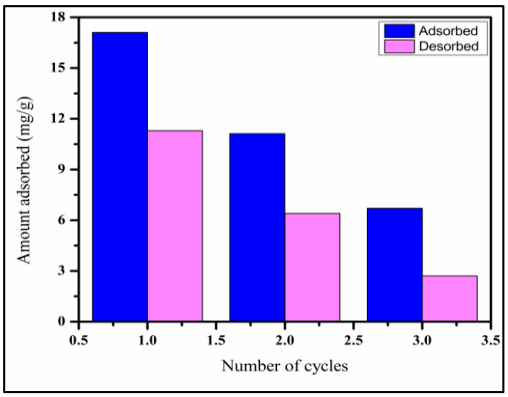

Figure 4.25 Regeneration - Cu(II)

4.10 Adsorption Isotherms

Adsorption isotherm is indicative of the distribution of adsorbate molecules among the solid and liquid phases at equilibrium conditions[144]. The results of the experimental data verified for different isotherms are discussed.

The adsorption capacities and equilibrium concentration values for DB2, RR152 and Cu(II) systems as derived from batch experimental results and their corresponding data for Langmuir, Freundlich, Tempkin and DKR plots are listed in tables 4.11-4.13. It is invariably understood that the equilibrium concentrations are found to increase with initial concentrations of the sorbates in all systems.

Table 4.11 Equilibrium/ Isothermal Data- DB2

Conc. of dye Solutions (mg/L)	C_e	q_e	Ce/q_e	log C_e	log q_e	lnC_e	ln q_e	ε^2 X10^8
25	1.2	11.9	0.1008	0.0792	1.0755	0.1823	2.477	23.318
50	3.1	23.4	0.1325	0.4914	1.3692	1.1314	3.153	4.961
75	6.1	34.4	0.1773	0.7853	1.5366	1.8083	3.538	1.463
100	9.6	49.2	0.2124	0.9823	1.6551	2.2618	3.811	0.623
125	13.0	56.5	0.2301	1.1139	1.7520	2.5649	4.034	0.349
150	17.3	66.3	0.2609	1.2380	1.8215	2.8507	4.194	0.200

Table 4.12 Equilibrium/Isothermal Data - RR152

Conc. of dye Solutions (mg/L)	C_e	q_e	Ce/q_e	logC_e	logq_e	lnC_e	lnq_e	ε^2 X10^8
25	0.6	6.1	0.0984	-0.2218	0.7853	-0.5108	1.808	61.058
50	1.6	12.1	0.1321	0.2041	1.0832	0.4700	2.494	14.961
75	3.3	17.9	0.1841	0.5185	1.2535	1.1939	2.886	4.447
100	5.6	23.6	0.2374	0.7482	1.3727	1.7228	3.161	1.713
125	9.2	28.9	0.3179	0.9637	1.4615	2.2192	3.365	0.676
150	13.2	34.2	0.3858	1.1205	1.5341	2.5802	3.533	0.338

Table 4.13 Equilibrium/Isothermal Data - Cu(II)

Conc. of Metal Solutions (mg/L)	C_e	q_e	C_e/q_e	$\log C_e$	$\log q_e$	$\ln C_e$	$\ln q_e$	$\varepsilon^2 X10^8$
4	0.033	3.3	0.0100	-1.4815	0.5193	-3.4112	1.196	652.6
8	0.126	6.4	0.0197	-0.8983	0.8078	-2.0683	1.860	403.6
12	0.326	9.4	0.0346	-0.4870	0.9740	-1.1215	2.243	225.0
16	0.524	12.9	0.0407	-0.2805	1.1103	-0.6459	2.556	72.3
20	1.154	17.1	0.0674	0.0621	1.2333	0.1430	2.840	24.7

4.10.1 Langmuir Isotherm

Langmuir plot (C_e/q_e vs C_e) shown in figures 4.26 and 4.27 for dyes and Cu(II) respectively are found to be straight lines. Langmuir constants q_m and b were calculated (as per the equation 11) from the slopes and intercepts of the obtained linear plots and these values listed in table 4.14 (DB2: 55.1 mg/g; RR152: 25.45 mg/g and Cu(II): 20.83 mg/g) reveal a saturated monolayer sorption. The calculated constants favour the better sorption nature of the current study than those reported for walnut and poplar woods activated carbons[145]. The favourability of sorption characteristics for the experimentally verified systems is further supported by the calculated correlation coefficient values ($R^2 \simeq 0.99$) and separation factor $R_L (0<R_L<1)$.

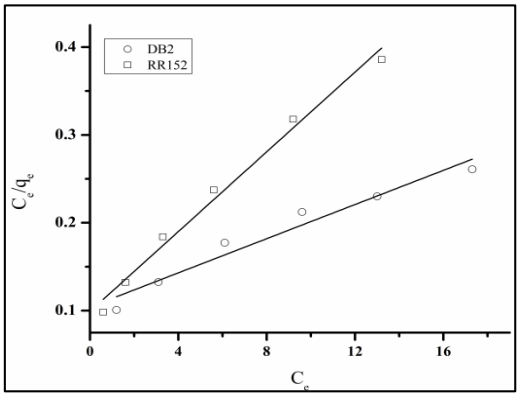

Figure 4.26 Langmuir Plot - DB2 & RR152

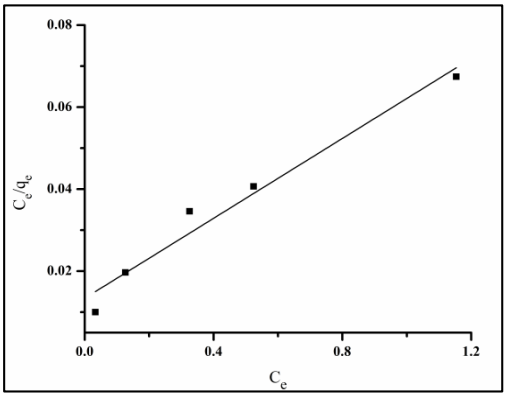

Figure 4.27 Langmuir Plot - Cu(II)

4.10.2 Freundlich Isotherm

The Freundlich constants K_F and 1/n (from equation 14) corresponding sorption capacities and sorption intensities derived from the intercepts and slopes of the Freundlich plot (log q_e versus log C_e) (Figure 4.28) are given in table 4.14. Higher K_F and smaller 1/n values favour greater sorption capacity[146]. Approximity in the R^2 values to unity and linearity favour lesser multilayer adsorption.

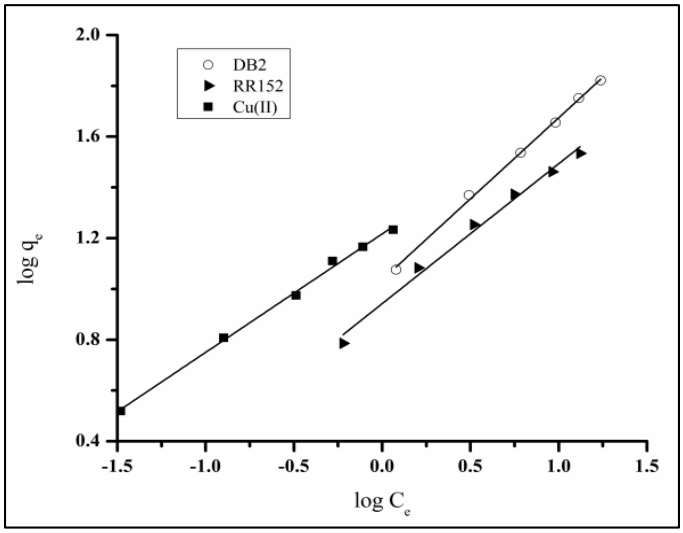

Figure 4.28 Freundlich Plot

4.10.3 Tempkin Isotherm

Tempkin isotherm takes into account the interactions between adsorbent and sorbate molecules and is based on the assumption that the free energy of sorption is a function of the surface coverage. The Tempkin constants A_T (equilibrium binding constant corresponding to the maximum binding energy) and b_T (Temkin isotherm constant) from equation (15) were derived from the intercepts and slopes of the linear plots (q_e vs ln C_e) illustrated in figure 4.29 and the calculated constants are listed in table 4.14. Correlation coefficient values pertaining the dyes and metal systems are calculated as 0.96 which indicates the applicability of this model for the systems.

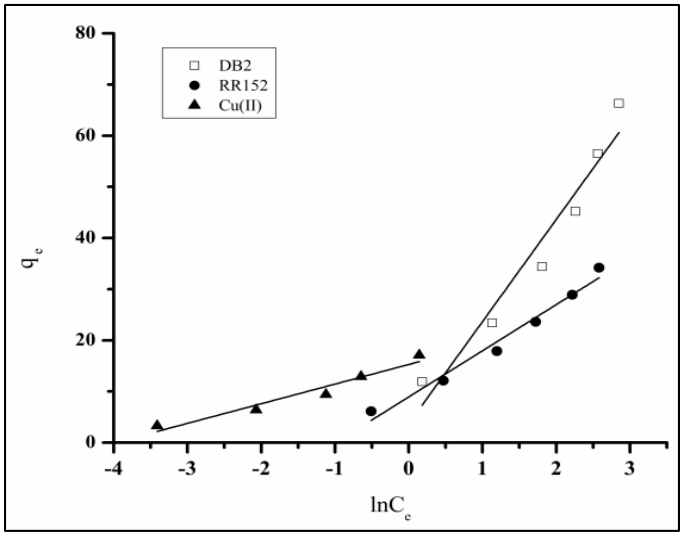

Figure 4.29 Tempkin Plot

4.10.4 Dubinin–Kaganer-Radushkevich (DKR) Isotherm

Three plots (ε^2 vs lnq_e) are depicted in figures 4.30-4.32 based on ε^2 values. From the straight lines obtained, the DKR constants q_s (saturation sorption capacity), β_{DR} (constant related to mean free energy) and E (mean free energy) were calculated for the three systems using equations (16 and 17) and listed in Table 4.14. E < 10 (2.817, 4.56 and 5.36 KJ/mol) indicate the predominance of physisorption[147].

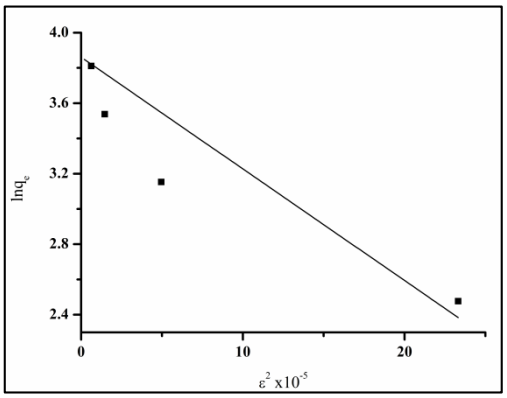

Figure 4.30 DKR Plot - DB2-PJBAC

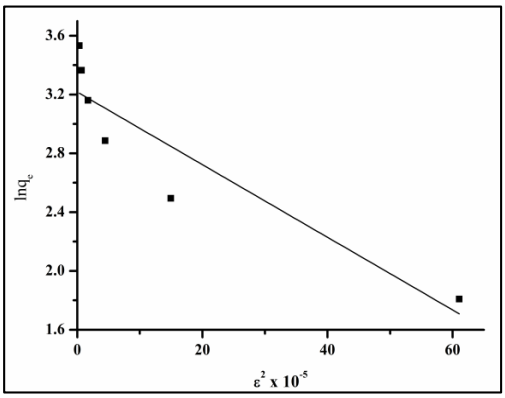

Figure 4.31 DKR Plot - RR152-PJBAC

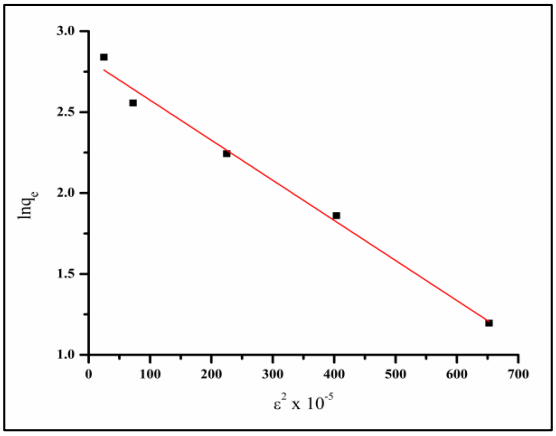

Figure 4.32 DKR Plot - Cu(II)-PJBAC

Table 4.14 Isothermal Constants

Isotherm Parameters	DB2	RR152	Cu(II)
Langmuir Isotherm			
q_m (mg/g)	55.1	25.45	20.83
b (L/g)	0.0865	0.2222	3.6929
R^2	0.9987	0.9985	0.9964
Freundlich Isotherm			
K_F (mg/g)	10.864	4.0045	16.44
n	1.5674	1.0189	2.1459
R^2	0.9580	0.9880	0.9681
Tempkin Isotherm			
A_T (L/g)	1.8189	1.3106	1.1217
b_T	126.2	279.09	657.1
R^2	0.9487	0.9771	0.9473
DKR Isotherm			
q_s (mg/g)	24.94	25.21	09.6
E (kJ/mol)	2.817	4.561	5.364
R^2	0.874	0.845	0.987

4.10.5 Comparison of Isotherm Models

Higher Isothermal constant values (q_m) exhibiting the better sorption capacity was observed in Langmuir model for the three chosen systems. The order of preference in comparison revealed Freundlich constant K_F followed by DKR constant q_s. Monolayer adsorption is also favoured by the A_T and b_T values (Tempkin Constants). This proved the better sorption capacity of PJBAC in trapping dyes/metal ion molecules where both monolayer sorption and heterogeneous surface conditions existed under the experimental conditions imbibing more than one mechanism[147].

4.11 Kinetic Studies

The mechanism of adsorption depends on the physical and chemical characteristics of the adsorbent as well as on the mass transfer process. The rate constants for the systems were calculated using pseudo-first-order and pseudo-second-order kinetic models suggested by Lagergren and Ho/McKay respectively and the rate controlling step was determined by intra-particle diffusion model.

4.11.1Pseudo-first-order model

The kinetic data for pseudo-first-order model are given in tables 4.15-4.17 and the corresponding linear plots are depicted in figures 4.33-4.35 for DB2, RR152 and Cu(II) systems. These plots of log (q_e–q_t) versus t resulted in a straight lines, where equilibrium adsorption capacities q_e and the first- order rate constants k_1 (from equation 18) were calculated (Table 4.18) from the intercepts and gradient of the lines, respectively[148].

4.11.2 Pseudo-second-order model

Tables 4.15 and 4.17 correspondingly lists out the experimental values for DB2, RR152 and Cu(II) systems. Linear plots of t/qt versus t (Figures 4.36-4.38) exhibited straight lines and q_e and k_2 (as per the equation 19) are calculated from gradient and intercepts of the lines respectively[149]. The calculated kinetic parameters, the sum of squares of errors (SSE) (using equation 20) and the correlation coefficients are shown in table 4.18. A relatively higher value of correlation coefficients as from the plots and lower values of SSE reveal the best fit of kinetic models[150].

The increase in q_e with concentration may be due to the efficient utilization of sorbents due to greater driving force[151]. An increase in the initial concentration of sorbate species reduces the diffusion of them in the boundary layers, k_2 (Pseudo second order rate constant) is observed to decreases with increase in initial concentration[152,153]. The above statements are in accordance with the research findings of Gupta[154] et al., and Ozgul Gercel[155] et al.

The correlation coefficients for pseudo-second-order model are relatively higher and the equilibrium sorption capacities determined using this model are in agreement with the experimentally determined equilibrium sorption capacities. The values of SSE are also less for pseudo-second-order model. Therefore, from the observations made the pseudo-second-order adsorption model is more suitable to describe the adsorption kinetics of the systems.

Table 4.15 Sorption Kinetics - DB2

Time (min)	50 (mg/L)		100 (mg/L)		150 (mg/L)	
	log (q_e-q_t)	**t/q_t**	**log (q_e-q_t)**	**t/q_t**	**log (q_e-q_t)**	**t/q_t**
10	1.504	0.313	1.820	0.151	2.015	0.097
20	1.496	0.639	1.806	0.313	2.007	0.197
30	1.479	0.995	1.795	0.481	1.998	0.301
40	1.465	1.369	1.780	0.664	1.980	0.419
50	1.443	1.801	1.763	0.863	1.963	0.545
60	1.424	2.259	1.739	1.095	1.922	0.717

Adsorbent dose: 100 mg; pH: 6; Temperature: 303K

Table 4.16 Sorption Kinetics - RR152

Time (min)	50 (mg/L)		100 (mg/L)		150 (mg/L)	
	log (q_e-q_t)	**t/q_t**	**log (q_e-q_t)**	**t/q_t**	**log (q_e-q_t)**	**t/q_t**
10	1.613	1.108	1.909	0.531	2.085	0.352
15	1.604	1.523	1.906	0.773	2.078	0.492
20	1.592	1.827	1.899	0.963	2.072	0.624
25	1.590	2.254	1.891	1.122	2.071	0.772
30	1.579	2.477	1.883	1.272	2.064	0.877

Adsorbent dose: 150 mg; pH: 6; Temperature: 303K

Table 4.17 Sorption kinetics - Cu(II)

Time (min)	4 (mg/L)		12 (mg/L)		20 (mg/L)	
	log (q_e-q_t)	**t/q_t**	**log (q_e-q_t)**	**t/q_t**	**log (q_e-q_t)**	**t/q_t**
3	-0.056	0.961	0.437	0.324	0.961	0.276
6	-0.074	1.900	0.420	0.640	0.862	0.472
9	-0.086	2.831	0.412	0.956	0.786	0.648
12	-0.109	3.724	0.385	1.254	0.760	0.843
15	-0.146	4.566	0.373	1.556	0.707	1.007
18	-0.159	5.445	0.356	1.850	0.633	1.146
21	-0.160	6.349	0.355	2.157	0.635	1.339

Adsorbent dose: 60 mg; pH: 6; Temperature: 303K

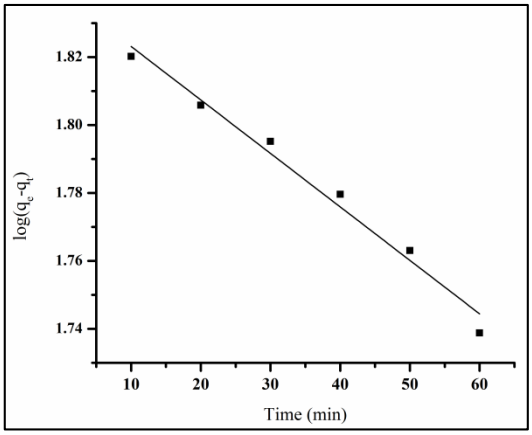

Figure 4.33 First order kinetics - DB2

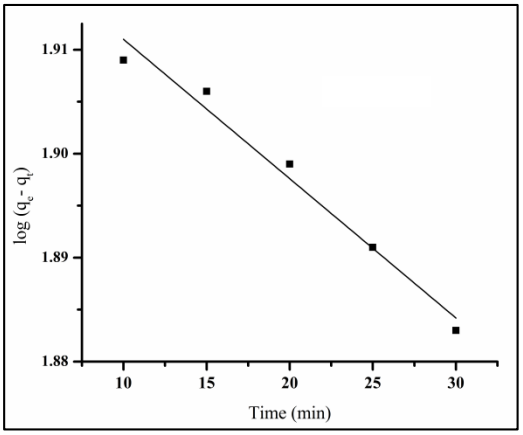

Figure 4.34 First order kinetics-RR152

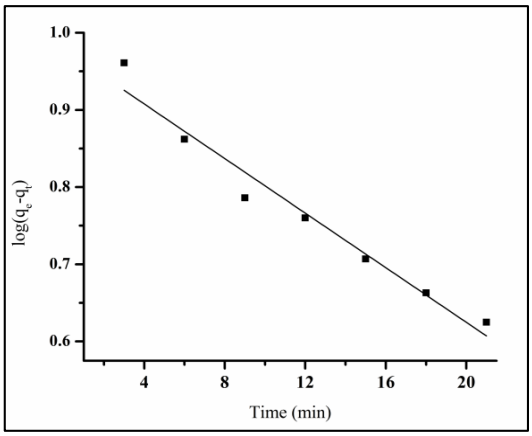

Figure 4.35 First order kinetics-Cu(II)

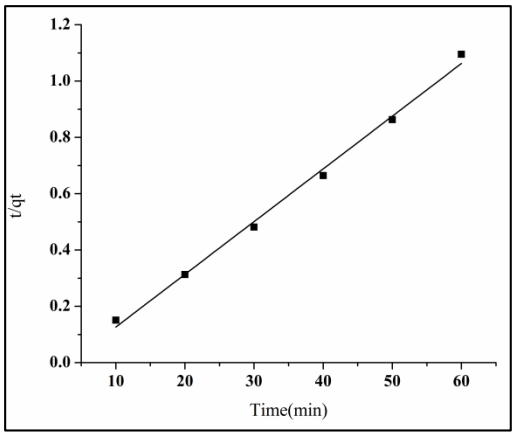

Figure 4.36 Second order kinetics-DB2

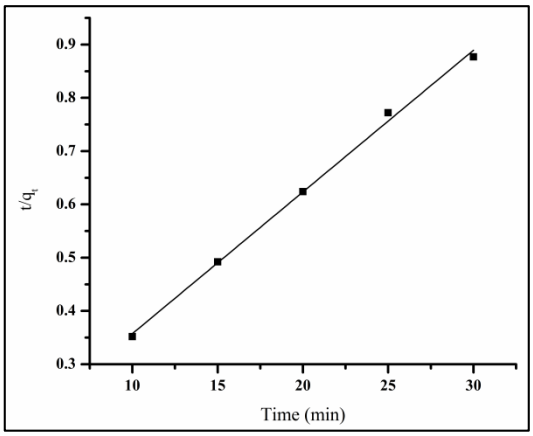

Figure 4.37 Second order kinetics - RR152

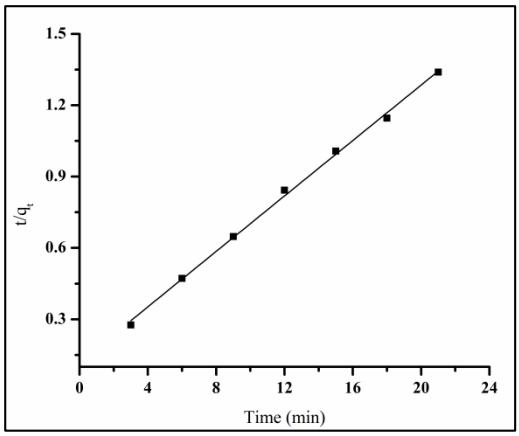

Figure 4.38 Second order kinetics -Cu(II)

Table 4.18 Comparison of Pseudo-first-order/ Pseudo-Second-order Kinetic Constants

Conc. of Dye/ Metal Ions (mg/L)	q_e exp. (mg/g)	Pseudo-first-order kinetics				Pseudo-second-order kinetics			
		q_e cal. (mg/g)	$k_1 \times 10^{-3}$ (min^{-1})	R^2	SSE	q_e cal. (mg/g)	$k_2 \times 10^{-4}$ (g/ mg min)	R^2	SSE
DB2									
50	23.4	12.92	0.1785	0.9801	6.30	25.74	0.004	0.9947	2.98
100	55.2	26.35	0.0875	0.9781	8.97	53.42	0.002	0.9913	4.72
150	66.3	39.13	0.0589	0.8949	9.30	72.03	0.001	0.9875	7.32
RR152									
50	12.11	7.521	0.3062	0.7062	5.17	14.49	0.011	0.9913	2.18
100	23.59	15.94	0.144	0.9621	6.27	27.77	0.009	0.9893	4.42
150	34.21	23.56	0.098	0.9347	11.13	38.46	0.006	0.9977	6.32
Cu(II)									
4	3.367	2.701	4.606	0.9221	1.61	3.306	0.824	0.9991	0.70
12	9.901	4.602	6.429	0.9321	3.80	9.419	0.375	0.9990	2.04
20	17.24	8.636	7.895	0.9143	6.27	17.11	0.029	0.9987	3.13

4.11.3 Comparison of Kinetic Models

The calculated and experimentally determined q_e values are significantly different from each other for pseudo first order, therefore the values are beyond comparison. But in the case of pseudo second order kinetic model the equilibrium sorption capacities (q_e) are in good agreement with experimentally determined q_e values, hence are comparable. Thence, pseudo second order kinetic model describes the systems in a better fashion. Similar results were observed for the adsorption studies of direct dyes onto activated carbons derived from saw dust[156] and palm ash[157].

4.11.4 Elovich Model

Elovich plots between (q_t and ln t) for the adsorption systems [DB2, RR152 and Cu(II)] at various initial concentrations are shown in figure 4.39. Elovich constants α and β corresponding to the initial adsorption rate and desorption constant were derived from the slopes and intercepts of the respective straight lines (Table 4.19 and 4.20). The adsorption rate (α) increases with initial dyes/metal ion concentrations from 25 to 150 mg/L and 4 to 20 mg/L respectively. Similarly, diminished β values at higher initial concentrations reveal the decline in the number of active sites available for the sorption process, thereby decline in the extent of surface coverage.

Table 4.19 Elovich Constants - DB2 & RR152

Conc. of Dye Solution (mg/L)	DB2 – PJBAC			RR152 – PJBAC		
	α	**β**	**R^2**	**α**	**β**	**R^2**
25	5.936	1.354	0.8791	0.3582	1.8093	0.8708
50	10.53	0.936	0.9688	2.6978	1.7027	0.9518
75	14.98	0.410	0.9800	4.9519	1.6573	0.9475
100	19.15	0.869	0.9672	8.1680	1.3765	0.9913
125	22.40	0.213	0.8508	14.100	0.9741	0.8091
150	22.75	0.797	0.8134	16.991	0.9586	0.9645

α: (mg/g min), β: (g/mg)

Table 4.20 Elovich Constants - Cu(II)

Conc. of Metal Solution (mg/L)	Cu(II)		
	α	**β**	**R^2**
4	2.985	1.103	0.921
8	6.426	0.943	0.908
12	8.935	0.756	0.946
16	7.609	0.413	0.964
20	8.343	0.419	0.983

α: (mg/g min), β: (g/mg)

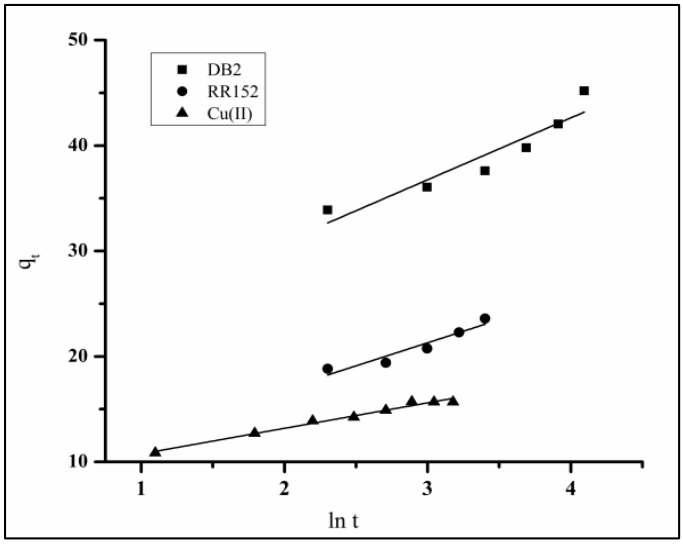

Figure 4.39 Elovich Plot

4.11.5 Intraparticle Diffusion Method

Two distinct phases obvious from the intraparticle diffusion plots (q_t versus $t^{1/2}$) are depicted in figures 4.40-4.42 which corresponds to surface sorption followed by intraparticle diffusion[158]. The first phase of the plot indicates a boundary layer diffusion effect while the second linear portion is due to the intraparticle or pore diffusion. The intraparticle diffusion parameter (K_i) and the boundary layer thickness (C) were calculated from the slopes and intercepts of the plots respectively (Table 4.21 and 4.22). The larger the intercept, the greater will be the contribution of the surface sorption towards the rate limiting step. The rate constants of intraparticle diffusion mechanism are found to increase with aqueous solutions concentrations.

Table 4.21 Intraparticle Diffusion Constants - DB2 & RR152

Conc of Dye Solution mg/L	DB2			RR152		
	K_i (mg/g $min^{1/2}$)	C	R^2	K_i (mg/g $min^{1/2}$)	C	R^2
25	8.807	0.101	0.9907	2.87	0.206	0.9741
50	16.657	0.221	0.9864	7.64	0.296	0.9663
75	24.220	0.329	0.9877	11.46	0.418	0.9632
100	31.430	0.438	0.9859	16.00	0.496	0.9811
125	37.350	0.547	0.8975	21.11	0.461	0.7063
150	40.703	0.763	0.9150	26.09	0.540	0.9591

Table 4.22 Intraparticle Diffusion Constants - Cu(II)

Conc of Metal Ion mg/L	Cu(II) – PJBAC		
	K_i (mg/g $min^{1/2}$)	C	R^2
4	1.930	0.157	0.358
8	4.029	0.296	0.312
12	5.742	0.458	0.348
16	6.052	0.734	0.544
20	7.018	0.935	0.590

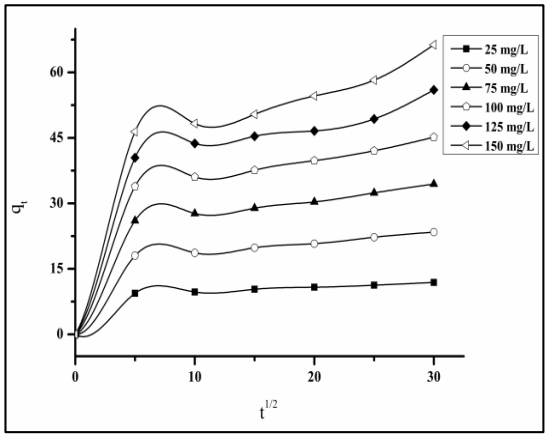

Figure 4.40 Intraparticle Diffusion Model - DB2

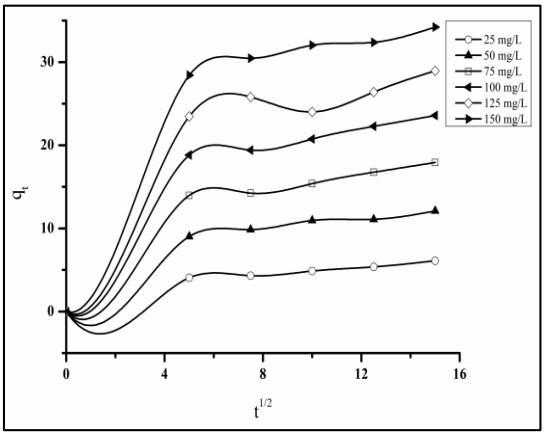

Figure 4.41 Intraparticle Diffusion Model - RR152

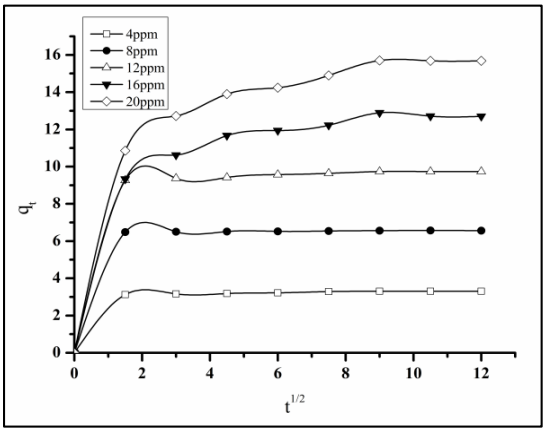

Figure 4.42 Intraparticle Diffusion Model -Cu(II)

4.12 Thermodynamic and Equilibrium Studies

Van't Hoff's plot (ln K_C vs. 1/T) as depicted in figure.4.43 furnish the thermodynamic constant values ΔH^o and ΔS^o from the slopes and intercepts. Free energy change (ΔG^o) was calculated using equation (25). The positive values of ΔS^o and negative values of ΔH^o and ΔG^o, evident from table 4.28 indicate the spontaneity, exothermicity and better feasibility of the systems. The negative values of ΔH^o suggested the exothermic nature of the process and lower ΔH^o values (<10kJ/mol) indicates physical adsorption to be a predominant mechanism in the adsorption process, favoured by the decrease in sorbate removal at higher temperatures[159]. Similar trend was observed for the adsorption of Crystal Violet onto NaOH-modified rice husk[160].

Table 4.23 Thermodynamic Constants

Temp (K)	DB2			RR152			Cu(II)		
	$-\Delta G^o \times 10^{-3}$ kJ/mol	ΔH^o kJ/mol	ΔS^o kJ/mol	$-\Delta G^o \times 10^{-3}$ kJ/mol	ΔH^o kJ/mol	ΔS^o kJ/mol	$-\Delta G^o \times 10^{-3}$ kJ/mol	ΔH^o kJ/mol	ΔS^o kJ/mol
303	0.2890			0.3612			0.6577		
313	0.3236	- 0.968	1.785	0.3494	-1.422	3.239	0.4979	-6.115	17.61
323	0.3572			0.3100			0.3304		
333	0.3969			0.2839			0.2278		

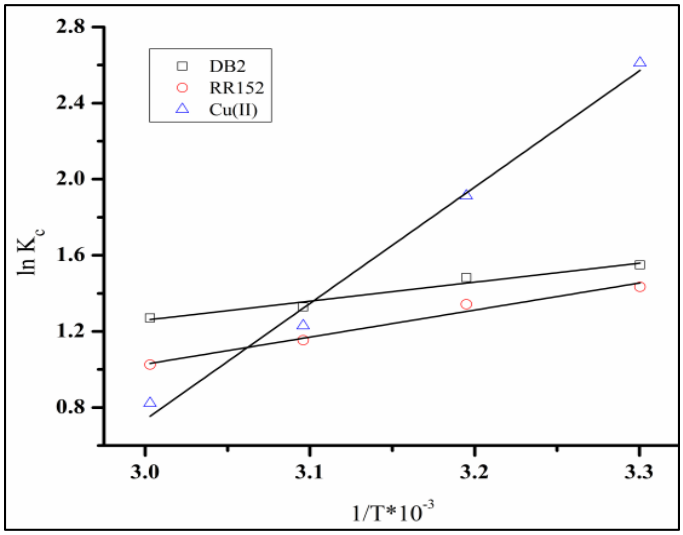

Figure 4.43 Vant Hoff's Plot